nature physics

LETTERS

PUBLISHED ONLINE: 13 MARCH 2017 | DOI: 10.1038/NPHYS4062

Waveform measurement of charge- and spin-density wavepackets in a chiral Tomonaga–Luttinger liquid

M. Hashisaka[1]*, N. Hiyama[1], T. Akiho[2], K. Muraki[2] and T. Fujisawa[1]*

In contrast to a free-electron system, a Tomonaga–Luttinger (TL) liquid in a one-dimensional (1D) electron system hosts charge and spin excitations as independent entities[1–4]. When an electron is injected into a TL liquid, it transforms into charge- and spin-density wavepackets that propagate at different group velocities and move away from each other. This process, known as spin–charge separation, is the hallmark of TL physics. While spin–charge separation has been probed in momentum- or frequency-domain measurements in various 1D systems[5–9], waveforms of separated excitations, which are a direct manifestation of the TL behaviour, have been long awaited to be measured. Here, we present a waveform measurement for the pseudospin-charge separation process in a chiral TL liquid comprising quantum Hall edge channels[9–13]. The charge- and pseudospin-density waveforms are captured by utilizing a spin-resolved sampling scope that records the spin-up or -down component of the excitations. This experimental technique provides full information for time evolution of the 1D electron system, including not only propagation of TL eigenmodes but also their decay in a practical device[14].

Co-propagating spin-up and -down edge channels of the quantum Hall (QH) state at filling factor $\nu = 2$ form a prototypical system for the study of TL physics. The TL eigenmodes have been identified by measuring interference of density waves[9], shot noise generation[10–12], and charge-density correlation between two paths in a Hong–Ou–Mandel experiment[13]. Dynamics of the charge- and spin-density excitations, that is, their excitation, propagation, and attenuation, are elementary processes of non-equilibrium phenomena in the 1D system. For investigating these processes, a waveform measurement for each density excitation is highly desirable. In this study, we developed a spin-resolved sampling scope comprising a spin filter and a time-resolved charge detector[15,16], which enables one to perform the waveform measurement. We actually observe charge- and pseudospin-density excitations separated over a distance exceeding 200 μm. The TL parameters (group velocities of charge- (v_C) and pseudospin-density ($v_S \leq v_C$) waves and mixing angle θ, which is introduced later) are directly read out from the waveforms; this is the first experiment in which all the TL parameters are estimated from a single measurement. Moreover, attenuation of TL wavepackets is evaluated from distortion of the waveforms. These results give quantitative information on various non-equilibrium phenomena in QH edge channels—for example, heat transport[17–20] and decoherence in interferometers[21,22].

The 1D electron dynamics in the co-propagating channels are formulated by the wave equation for the spin-up and -down charge densities $\rho_{\uparrow,\downarrow}(x,t)$[23–25]

$$\frac{\partial}{\partial t}\begin{pmatrix}\rho_\uparrow\\ \rho_\downarrow\end{pmatrix} = -\mathbf{U}\frac{\partial}{\partial x}\begin{pmatrix}\rho_\uparrow\\ \rho_\downarrow\end{pmatrix} = -\begin{pmatrix}v_\uparrow & U_X\\ U_X & v_\downarrow\end{pmatrix}\frac{\partial}{\partial x}\begin{pmatrix}\rho_\uparrow\\ \rho_\downarrow\end{pmatrix}$$

where U_X is the inter-channel interaction and $v_\uparrow$ ($v_\downarrow$) is the group velocity renormalized by the intra-channel interaction in the spin-up (down) channel. While conventional TL theory assumes $v_\uparrow = v_\downarrow$, we consider a more general case wherein they can differ, taking geometric asymmetry of the channels into account. By diagonalizing the matrix $\mathbf{U}$, we obtain transport eigenmodes: the charge mode $\boldsymbol{\rho}_C = (\rho_{C\uparrow}, \rho_{C\downarrow}) = (\cos\theta, \sin\theta)$ and the pseudospin mode (sometimes called dipole or neutral mode; in the following we call it 'spin mode' for short) $\boldsymbol{\rho}_S = (\rho_{S\uparrow}, \rho_{S\downarrow}) = (\sin\theta, -\cos\theta)$[9,10,13]. The mixing angle $\theta(0 \leq \theta \leq \pi/2)$ represents the asymmetry between the two channels. Pure spin–charge separation ($\theta = \pi/4$) occurs for the symmetric case with $v_\uparrow = v_\downarrow$.

A schematic of the measurement is shown in Fig. 1. We focus on the co-propagating channels labelled 'target channels' in the

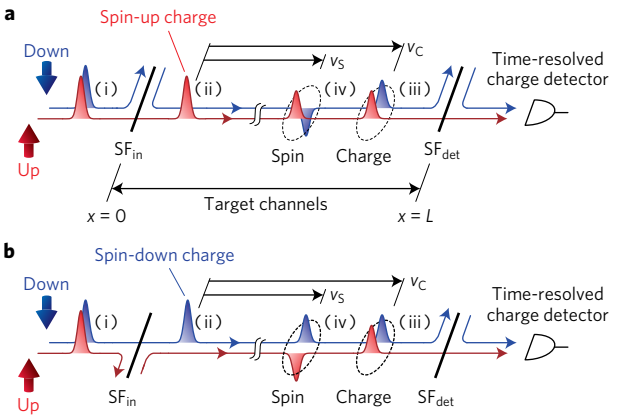

Figure 1 | Principle of the experiment. a, Spin-up charge injection into the target channels through SF_{in}. The spin-up charge components of separated charge and spin excitations are extracted through SF_{det} and are detected by the time-resolved charge detector. A pair of same-charge-polarity peaks should be detected. **b**, Spin-down charge injection. Peak and dip structure should be detected in this case.

[1]Department of Physics, Tokyo Institute of Technology, 2-12-1-H81 Ookayama, Meguro, Tokyo 152-8551, Japan. [2]NTT Basic Research Laboratories, NTT Corporation, 3-1 Morinosato-Wakamiya, Atsugi, Kanagawa 243-0198, Japan. *e-mail: hashisaka@phys.titech.ac.jp; fujisawa@phys.titech.ac.jp

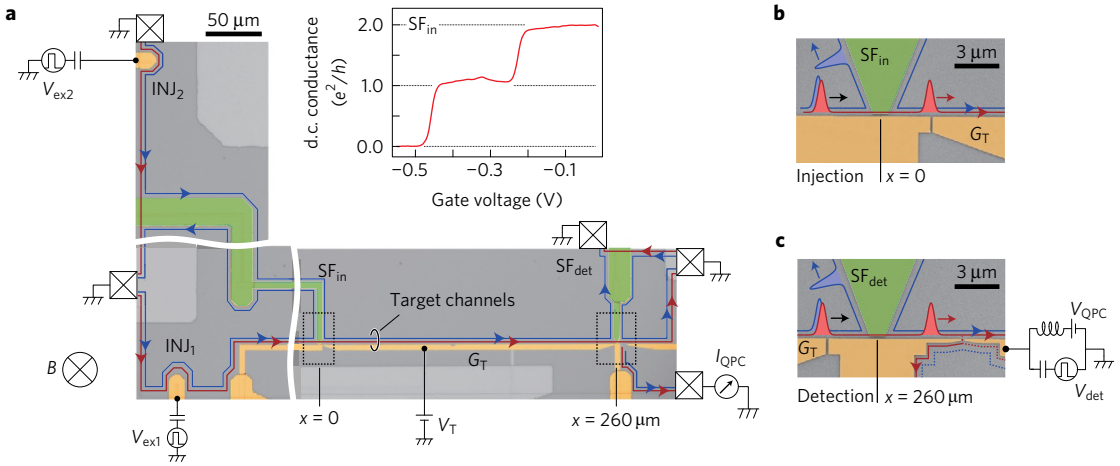

Figure 2 | Experimental set-up. a, Coloured optical micrograph of the sample fabricated on an AlGaAs/GaAs heterostructure. The 2DES under the yellow gates is completely depleted. The green gates are used to form SF_{in} and SF_{det}. An initial charge-mode packet is excited through capacitive coupling by a 4.2-mV step voltage V_{ex1} or V_{ex2} applied to the injector gate INJ_1 or INJ_2, respectively. (Inset, d.c. pinch-off trace of SF_{in}.) Spin filtering is confirmed in a wide e^2/h plateau. To activate SF_{in}, the gate voltage is set at −0.32 V. **b**, Magnified view near the injection point ($x = 0$). **c**, Magnified view near the detection point ($x = 260\,\mu m$). The detector QPC is opened temporarily by the voltage pulse V_{det} of amplitude 7.1 mV and width 100 ps.

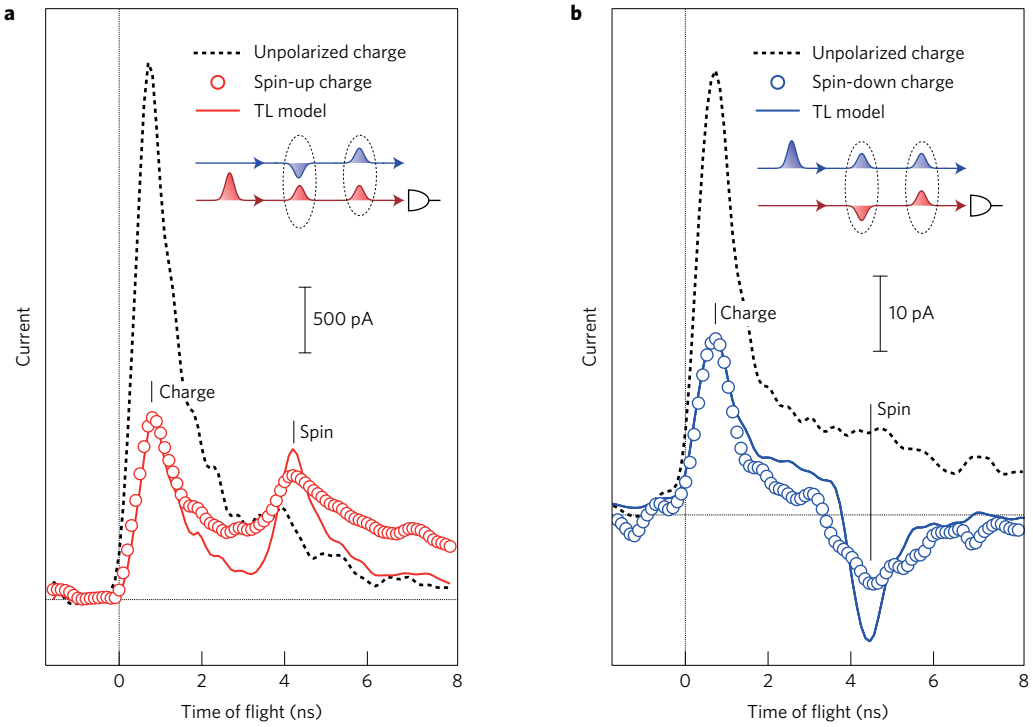

Figure 3 | Representative experimental results. a,**b**, Representative waveforms measured at $V_T = -2.0$ V as a function of time of flight along the channels. Insets show the schematic of the measurements. Red circles in **a**: waveform obtained with spin-up charge ($d(t)$, 0) injection. Blue circles in **b**: waveform measured with spin-down charge (0, $d(t)$) injection. Black dashed lines: waveforms obtained with unpolarized-charge injections. Solid lines: simulated curves using the parameters $v_\uparrow \cong 330\,km\,s^{-1}$, $v_\downarrow \cong 210\,km\,s^{-1}$ and $U_X \cong 200\,km\,s^{-1}$. The data in **a** and **b** are measured with different cooldowns for rewiring radio frequency signal lines.

figure. First, an initial charge-mode wavepacket (i) is excited and fed to the spin filter SF_{in} placed at the entrance of the target channels ($x = 0$). A spin-up (Fig. 1a) or -down (Fig. 1b) charge packet (ii) is injected through SF_{in} by filtering out the other spin component. The spin-polarized charge packet splits into charge- and spin-mode packets (iii and iv), which are spatially separated after propagation. Each separated packet is decomposed by the second spin filter SF_{det} placed in front of the time-resolved detector ($x = L$). Only the spin-up charge components are measured to construct the objective waveforms.

Time evolution of a spin-polarized charge packet induced at $x = 0$, for example, spin-up charge ($d(t)$, 0), is described as a superposition of the two modes

$$\boldsymbol{\rho}(x,t) = \cos\theta\,\boldsymbol{\rho}_C d(t - x/v_C) + \sin\theta\,\boldsymbol{\rho}_S d(t - x/v_S)$$

where $d(t)$ is the real-time charge distribution function centred at $t = 0$. We measure the spin-up component $\rho_\uparrow(L, t)$. In an ideal TL liquid, $\boldsymbol{\rho}_C$ and $\boldsymbol{\rho}_S$ propagate without attenuation; thus, v_C, v_S and θ (and thus $v_\uparrow$, $v_\downarrow$ and U_X) are directly extracted from the waveforms.

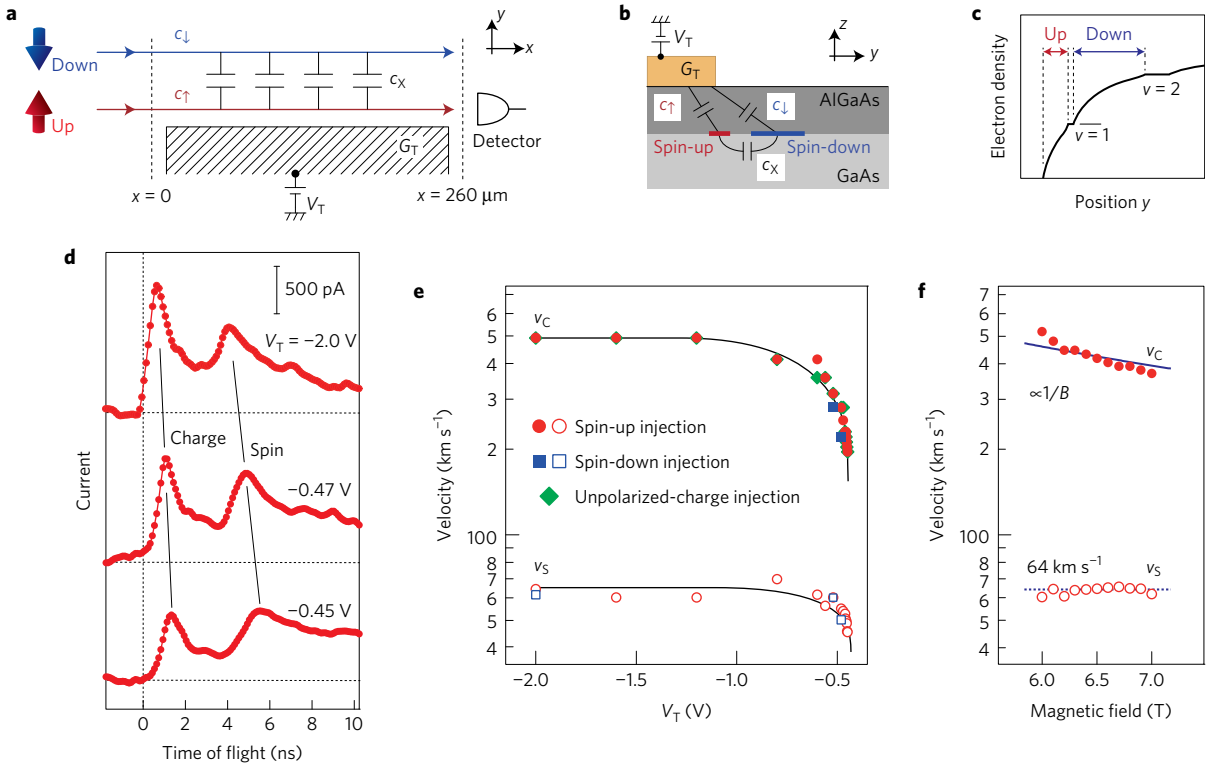

Figure 4 | Tuning transport properties. a, Distributed-element circuit model of target channels. **b**, Schematic cross-section of the target channels. **c**, Schematic of the electron-density profile at the edge of the 2DES. **d**, Representative waveforms with spin-up charge injection measured at $B = 6.5$ T and at $V_T = -2.0$, -0.47 and -0.45 V. **e**, V_T dependences of v_C (filled) and v_S (open symbols). Solid black lines are visual guides. **f**, Magnetic field B dependences of v_C and v_S measured at $V_T = -2.0$ V. The velocity v_C varies following the $1/B$ curve (solid line), while v_S remains nearly constant at 64 km s^{-1} (dotted line).

In an actual 1D electron system, attenuation of these eigenmodes results in distortion of the waveforms from which deviation from the TL behaviour can be evaluated.

Figure 2a shows the experimental set-up and optical micrograph of the device. The measurement was performed at 320 mK in a magnetic field $B = 6.5$ T ($\nu = 2$) applied perpendicular to the 2D electron system (2DES). Spin-up and -down edge channels (indicated by red and blue lines, respectively) are formed along the energized surface gates (green and yellow patterns). We focus on the 260-μm target channels along gate G_T, which are formed by applying a gate voltage V_T to completely deplete 2DES under the gate.

An initial charge-mode packet is excited at the injector gates INJ_1 or INJ_2 by applying step voltages V_{ex1} or V_{ex2}, respectively[15]. The spin filters SF_{in} and SF_{det} comprise local QH regions at $\nu = 1$ formed under the gates, where only the spin-up channels travel through the gated regions (inset in Fig. 2a). When the initial packet is fed from INJ_1 (INJ_2), a spin-up (-down) charge packet is injected into the target channels (Fig. 2b). The spin-polarized charge packet splits into charge- and spin-mode packets, which are measured at different timings by the detector comprising SF_{det} and the quantum point contact (QPC) (Fig. 2c)[15,16].

The circles in Fig. 3a,b represent the central results obtained when spin-up and -down charge packets are injected, respectively. We observe the first peaks at the time of flight (approximately 0.5 ns) as well as an additional peak in Fig. 3a and a dip in Fig. 3b at approximately 4 ns. The distinct spin dependence of the current polarity allows us to unambiguously identify the first and second features as the charge and spin modes, respectively. This is reconfirmed by comparing the data with the results of control experiments, where SF_{in} is deactivated. As the injected spin-unpolarized charge packet is an eigenmode in this case, a single peak is observed, indicating no spin–charge separation (dashed lines). The peak positions coincide with those of the first peaks in the spin-polarized charge injection case.

The clearly resolved peak–peak (peak–dip) structure is a manifestation of the long-range ballistic transport of the TL eigenmodes. This implies that the co-propagating channels are well described by the chiral TL-liquid theory. From the arrival times, we obtain $v_C \cong 480$ km s^{-1} and $v_S \cong 65$ km s^{-1}. The distance D between the excitations is estimated from these velocities. For example, $D \cong 225$ μm at the charge-mode detection timing (0.54 ns). The ratio of the charge- and spin-mode peak heights I_C and I_S, respectively, measured in case of the spin-up charge injection (Fig. 3a) provides the mixing angle $\theta \cong 0.2\pi$. From these results, we obtain the TL parameters as $v_\uparrow \cong 330$ km s^{-1}, $v_\downarrow \cong 210$ km s^{-1} and $U_X \cong 200$ km s^{-1}.

The solid lines in Fig. 3a,b represent the waveforms simulated using the obtained TL parameters without considering attenuation. In these calculations, $d(t)$ is determined assuming $d(t - L/v_C) \propto \rho_{0,\uparrow}(L, t)$, where $\rho_{0,\uparrow}(L, t)$ is the spin-up component of $\boldsymbol{\rho}(x, t)$ measured with the unpolarized-charge injections (dashed lines). The main features of the experiment and simulations agree fairly well. A small deviation in the shape of the spin-mode peaks indicates the presence of attenuation, particularly in spin-density waves, which is caused by inter-channel spin-flip tunnelling (Supplementary Information). Thus, an additional process that causes deviation from the TL model is identified from the obtained waveforms.

In the rest of this paper, we discuss tuning of the 1D electron dynamics. The transport properties of the TL eigenmodes depend on the surrounding environment, which screens the interactions in the channels[10,16]. The screening strengths are represented by distributed electrochemical capacitances $c_\uparrow$, $c_\downarrow$ and c_X as shown in Fig. 4a[24,25] (see Methods). Figure 4b,c shows a schematic

cross-section of the channels and the electron-density profile, respectively, at a filling factor slightly greater than $\nu = 2$. Compressible strips separated by the incompressible strip form the co-propagating channels[26]. The widths and positions of these strips vary with experimental parameters, resulting in the tuning of $c_\uparrow$, $c_\downarrow$ and c_X, and thus the TL parameters.

Figure 4d shows the waveforms for spin-up charge injection measured at several V_T values below the depletion voltage $V_{T,dep} = -0.44$ V. While the two-peak structures are observed in all traces, the shapes of the peaks vary with V_T. The group velocities v_C and v_S extracted from the peak positions are summarized in Fig. 4e. The velocities increase monotonically with decreasing V_T, reflecting the fact that the channels move apart from the gate metal, thereby reducing $c_\uparrow$ and $c_\downarrow$. The steep enhancement of the velocities at $-0.55\,\mathrm{V} < V_T < -0.45\,\mathrm{V}$ indicates the edge configurations that change rapidly in this V_T range.

The TL parameters can also be tuned by B. Figure 4f shows the B dependences of v_C and v_S near $\nu = 2$. While v_C varies following the curve $\nu \propto 1/B$ (solid line) corresponding to the theory of edge magnetoplasmon transport[27], v_S remains nearly constant at $64\,\mathrm{km\,s^{-1}}$. These behaviours are explained by considering asymmetric B dependences of the channel widths (Supplementary Information). In this manner, the TL behaviours are modified by the environmental parameters. The variety of such behaviours results in a wide range of non-equilibrium phenomena in QH systems.

Thus, we have presented a waveform measurement for the pseudospin–charge separation process. While this study focuses on the integer QH edge channels, the concept of decomposing TL eigenmodes can be used to investigate electron dynamics in various 1D systems; for example, neutral-mode transport in reconstructed edges in fractional QH systems[28].

Methods

Methods, including statements of data availability and any associated accession codes and references, are available in the online version of this paper.

Received 9 December 2016; accepted 13 February 2017; published online 13 March 2017

References

1. Tomonaga, S. Remarks on Bloch's method of sound waves applied to many-fermion problems. *Prog. Theor. Phys.* **5,** 544–569 (1950).
2. Luttinger, J. M. An exactly soluble model of a many-fermion system. *J. Math. Phys.* **4,** 1154–1162 (1963).
3. Haldane, F. D. M. 'Luttinger liquid theory' of one-dimensional quantum fluids. I. Properties of the Luttinger model and their extension to the general 1D interacting spinless Fermi gas. *J. Phys. C* **14,** 2585–2609 (1981).
4. Giamarchi, T. *Quantum Physics in One Dimension* (Oxford Univ. Press, 2004).
5. Auslaender, O. M. *et al*. Tunneling spectroscopy of the elementary excitations in a one-dimensional wire. *Science* **295,** 825–828 (2002).
6. Jompol, Y. *et al*. Probing spin-charge separation in a Tomonaga–Luttinger liquid. *Science* **325,** 597–602 (2009).
7. Bochrath, M. *et al*. Luttinger-liquid behaviour in carbon nanotubes. *Nature* **397,** 598–601 (1999).
8. Lorenz, T. *et al*. Evidence for spin–charge separation in quasi-one-dimensional organic conductors. *Nature* **418,** 614–617 (2002).
9. Bocquillon, E. *et al*. Separation of neutral and charge modes in one-dimensional chiral edge channels. *Nat. Commun.* **4,** 1839 (2013).
10. Inoue, H. *et al*. Charge fractionalization in the integer quantum Hall effect. *Phys. Rev. Lett.* **112,** 166801 (2014).
11. Berg, E., Oreg, Y., Kim, E.-A. & von Oppen, F. Fractional charges on an integer quantum Hall edge. *Phys. Rev. Lett.* **102,** 236402 (2009).
12. Neder, I. Fractionalization noise in edge channels of integer quantum Hall states. *Phys. Rev. Lett.* **108,** 186404 (2012).
13. Freulon, V. *et al*. Hong–Ou–Mandel experiment for temporal investigation of single-electron fractionalization. *Nat. Commun.* **6,** 6854 (2015).
14. Barak, G. *et al*. Interacting electrons in one dimension beyond the Luttinger-liquid limit. *Nat. Phys.* **6,** 489–493 (2010).
15. Kamata, H., Kumada, N., Hashisaka, M., Muraki, K. & Fujisawa, T. Fractionalized wave packets from an artificial Tomonaga–Luttinger liquid. *Nat. Nanotech.* **9,** 177–181 (2014).
16. Kamata, H., Ota, T., Muraki, K. & Fujisawa, T. Voltage-controlled group velocity of edge magnetoplasmon in the quantum Hall regime. *Phys. Rev. B* **81,** 085329 (2010).
17. Levkivskyi, I. P. & Sukhorukov, E. V. Energy relaxation at quantum Hall edge. *Phys. Rev. B* **85,** 075309 (2012).
18. le Sueur, H. *et al*. Energy relaxation in the integer quantum Hall regime. *Phys. Rev. Lett.* **105,** 056803 (2010).
19. Altimiras, C. *et al*. Tuning energy relaxation along quantum Hall channels. *Phys. Rev. Lett.* **105,** 226804 (2010).
20. Washio, K. *et al*. Long-lived binary tunneling spectrum in the quantum Hall Tomonaga–Luttinger liquid. *Phys. Rev. B* **93,** 075304 (2016).
21. Neder, I., Heiblum, M., Levinson, Y., Mahalu, D. & Umansky, V. Unexpected behavior in a two-path electron interferometer. *Phys. Rev. Lett.* **96,** 016804 (2006).
22. Levkivskyi, I. P. & Sukhorukov, E. V. Dephasing in the electronic Mach–Zehnder interferometer at filling factor $\nu = 2$. *Phys. Rev. B* **78,** 045322 (2008).
23. Wen, X. G. Gapless boundary excitations in the quantum Hall states and in the chiral spin states. *Phys. Rev. B* **43,** 11025–11036 (1991).
24. Hashisaka, M. *et al*. Distributed-element circuit model of edge magnetoplasmon transport. *Phys. Rev. B* **88,** 235409 (2013).
25. Hashisaka, M., Washio, K., Kamata, H., Muraki, K. & Fujisawa, T. Distributed electrochemical capacitance evidenced in high-frequency admittance measurements on a quantum Hall device. *Phys. Rev. B* **85,** 155424 (2012).
26. Chklovskii, D. B., Shklovskii, B. I. & Glazman, L. I. Electrostatics of edge channels. *Phys. Rev. B* **46,** 4026–4034 (1992).
27. Volkov, V. A. & Mikhailov, S. A. Edge magnetoplasmons: low frequency weakly damped excitations in inhomogeneous two-dimensional electron systems. *Sov. Phys. JETP* **67,** 1639–1653 (1988).
28. Bid, A. *et al*. Observation of neutral modes in the fractional quantum Hall regime. *Nature* **466,** 585–590 (2010).

Acknowledgements

The authors thank H. Kamata, N. Kumada and Y. Tokura for their beneficial discussions. This work was supported by Grants-in-Aid for Scientific Research (JP26103508, JP15H05854, JP26247051, JP16H06009) and the Nanotechnology Platform Program of the Ministry of Education, Culture, Sports, Science and Technology, Japan.

Author contributions

M.H. and T.F. designed and supervised this study. N.H. and M.H. performed the experiment and analysed the data. T.A. and K.M. grew the wafer. M.H. wrote the manuscript with help from T.F. and K.M. All authors discussed the results and commented on the manuscript.

Additional information

Supplementary information is available in the online version of the paper. Reprints and permissions information is available online at www.nature.com/reprints. Publisher's note: Springer Nature remains neutral with regard to jurisdictional claims in published maps and institutional affiliations. Correspondence and requests for materials should be addressed to M.H. or T.F.

Competing financial interests

The authors declare no competing financial interests.

Methods

Sample fabrication. We fabricated the sample in a standard AlGaAs/GaAs heterostructure with a two-dimensional electron gas located 95 nm below the surface having electron density of 3.0×10^{11} cm^{-2} and mobility of 1.0×10^{6} cm^{2} V^{-1} s^{-1}. The sample was patterned using photolithography for chemical etching and coarse metallized structures, as well as electron-beam lithography for fine gate structures. The ohmic contacts shown by the white squares with cross marks in Fig. 2a were formed by alloying Au–Ge–Ni onto the surface.

Time-resolved charge detection. This technique was performed by applying two radio frequency (RF) voltages. One is the square-wave voltage V_{ex1} or V_{ex2} (amplitude: 4.2 mV peak to peak, period: 40 ns) applied to the gate INJ_1 or INJ_2 to excite an initial charge packet. The other is the square pulse voltage V_{det} (amplitude: 7.1 mV peak to peak, width: 100 ps) for temporary opening of the quantum point contact (QPC). The initial charge packets are excited at the edge of the square wave. In this study, we focused on the positive charge packets excited at the rising edge. Note that the main results are reproduced with the opposite charge polarity on the negative charge packets excited at the falling edge. These RF voltages generate a charge flow through the QPC when the detection pulse synchronizes with the arrival of a charge excitation at the QPC. We measured the current I_{QPC} as a function of the time delay τ of the detection pulse from the excitation voltage, under successive applications of these voltages at a repetition frequency of 25 MHz.

We assume that the initial charge packet is spin unpolarized. While this is not the case when $\theta \neq \pi/4$ or when the capacitive coupling of the injection gate with the inner and outer channels are unequal, in the present experiment the deviation from this assumption is small and does not affect the main results. This can be confirmed in the waveforms without activating SF_{in} (dashed lines in Fig. 3a,b), where only single peaks are observed.

In this experiment, the time origin of the waveform measurement is defined as the moment of the spin-polarized charge excitation at $x = 0$. We estimated the moment in the I_{QPC} trace by the following procedure. First, we defined a straight channel from INJ_1 to the detector by applying -2.0 V to the gates (total length of the channels is $L_{total} = 560\,\mu$m). Second, an I_{QPC} trace was measured with the charge-mode packet injection at INJ_1 without activating SF_{in}. The arrival time τ_C of the packet at the detector was evaluated from the peak position. Then, the excitation timing τ_0 with charge injection at INJ_1 was calculated as $\tau_0 = \tau_C \times (L_{total} - L)/L_{total}$, where $L = 260\,\mu$m is the length of the target channels. With charge injection at INJ_2, we performed similar measurement to estimate arrival time τ'_C and calculated the excitation timing as $\tau'_0 = \tau'_C - L/v_C$. In this way, we determined the time origins of the waveform measurements as τ_0 and τ'_0.

Distributed-element circuit model of co-propagating edge channels. Intra- and inter-channel Coulomb interaction in co-propagating edge channels can be modelled by distributed electrochemical capacitances[24,25]. Assuming the corresponding circuit model shown in Fig. 4a, the wave equation for charge excitations $\rho_\uparrow$ and $\rho_\downarrow$ described in the main text can be substituted by

$$\frac{\partial}{\partial t}\begin{pmatrix}\rho_\uparrow\\ \rho_\downarrow\end{pmatrix} = -\sigma_{xy}\begin{pmatrix}c_\uparrow + c_X & -c_X\\ -c_X & c_\downarrow + c_X\end{pmatrix}^{-1}\frac{\partial}{\partial x}\begin{pmatrix}\rho_\uparrow\\ \rho_\downarrow\end{pmatrix}$$

where $\sigma_{xy} = e^2/h$ is the Hall conductivity, $c_\uparrow$ ($c_\downarrow$) is the spin-up (-down) channel capacitance, and c_X is the inter-channel capacitance. The TL parameters $v_\uparrow$, $v_\downarrow$, and U_X can be expressed by using these capacitances as

$$v_\uparrow = \sigma_{xy}\frac{c_\downarrow + c_X}{c_\uparrow c_\downarrow + c_\uparrow c_X + c_\downarrow c_X}$$

$$v_\downarrow = \sigma_{xy}\frac{c_\uparrow + c_X}{c_\uparrow c_\downarrow + c_\uparrow c_X + c_\downarrow c_X}$$

$$U_X = \sigma_{xy}\frac{c_X}{c_\uparrow c_\downarrow + c_\uparrow c_X + c_\downarrow c_X}$$

By substituting the experimental results $v_\uparrow \cong 330$ km s^{-1}, $v_\downarrow \cong 210$ km s^{-1}, and $U_X \cong 200$ km s^{-1}, we obtain $c_\uparrow \cong 15$ pF m^{-1}, $c_\downarrow \cong 170$ pF m^{-1}, and $c_X \cong 240$ pF m^{-1}, which are comparable to the values in the case of counter-propagating edge channels[24,25].

Data availability. The data that support the plots within this paper and other findings of this study are available from the corresponding author upon reasonable request.